On-surface magnetocaloric effect for a Van der Waals Gd(III) 2D MOF grown on Si

Subodh Kumar,[a,b] Guillem Gabarró Riera,[a,b] Ana Arauzo,[c] Jakub Hrubý,[d] Stephen Hill,[d,e] Lapo Bogani,[f] Juan Rubio-Zuazo,[g,h] Jesús Jover,[a,i] Elena Bartolomé,*[j] E. Carolina Sañudo*[a,b]

[a] Institut de Nanociències i Nanotecnologia, Universitat de Barcelona (IN2UB), 08028 Barcelona, Spain
[b] Departament de Química Inorgànica i Orgànica, Secció de Química Inorgànica, C/Martí i Franqués 1-11, 08028, Barcelona, Spain
[c] Instituto de Nanociencia y Materiales de Aragón (INMA), CSIC-Universidad de Zaragoza, and Departamento de Física de la Materia Condensada, 50009 Zaragoza, Spain
[d] National High Magnetic Field Laboratory, Tallahassee, FL 32310, USA.
[e] Department of Physics, Florida State University, Tallahassee, FL 32306, USA.
[f] Department of Materials, University of Oxford, 16 Parks Road, OX1 3PH, Oxford, UK
[g] BM25-SpLine beamline at the ESRF, 71 Avenue des Martyrs, 38043, Grenoble, France
[h] Instituto de Ciencia de Materiales de Madrid-CSIC, Sor Juana Inés de la Cruz, 3, Cantoblanco, 28049 Madrid, Spain
[i] Institut de Química Teórica i Computacional (IQTC), Department of Inorganic and Organic Chemistry, Faculty of Chemistry, University of Barcelona
[j] Institut de Ciència de Materials de Barcelona (ICMAB), CSIC, Campus UAB, 08193 Barcelona, Spain

Contents:

Figure S5: Temperature dependent CW HF-EPR spectra of bulk **1**, recorded at 104 GHz and the temperatures given in the legend. Anisotropic spectral features span from 3.0 to 4.15 T (dotted vertical lines), corresponding to effective *g*-values, g^{eff} = 2.48 and 1.79, respectively. The dashed vertical line indicates the central m_S = -1/2 to 1/2 transition at g^{eff} = 1.985.

Figure S6: Comparison between experimental 104 GHz HF-EPR spectra and simulations obtained using the spin Hamiltonian of Eq. 1 (main text) at temperatures of 5 and 80 K.

Figure S7. Comparison between experimental 104 GHz HF-EPR spectra and simulations obtained using the MSH of Eq. S1, both for the FM (a) and AF (b) cases, with $J = \pm 0.025\ \mathrm{cm}^{-1}$ ($J/k_B = \pm 0.036$ K), (see legend).

Figure S8. (a) $\chi''(f, H)$ curves measured in the high frequency-region by PPMS at T = 2.0 K and different applied magnetic fields (0-1 T), where the presence of the two relaxation processes τ_2 and τ_3 are is observed; (b) field dependence of the relaxation times $\tau_2(H)$ and $\tau_3(H)$.

Figure S9. (a) Optical microscopy photograph of Gd 2D MOF flakes deposited on silicon by spin coating. (b) Field-dependence of the total magnetic moment, $m_{tot}(H)$, obtained from XMCD(H); a value m_{tot} = 6.7 ± 0.3 μ_B/ion was obtained from sum rules at 6 T and 3.4 K; the magnetization curve, $M(H)$, measured by SQUID magnetometer for **1** in bulk is also shown at the same temperature, along with the theoretically expected $m_{tot}(H)$ curve for a Brillouin function with g = 2 at 3.4 K.

Figure S10. Magnetic entropy change, $-\Delta S_m$, at the indicated field change for **1**.

Figure S11. Magnetization vs field as a function of temperature (2 to 10 K) for **1Si**.

Figure S12. (a) AFM image of **1Si** after 1 hour deposition time. Roughness is indicated in the figure. (b) AFM image and height profile for **1Si** at 24h deposition time., showing some large crystallites grafted on the TSP functionalized Si wafer. (c) AFM image and height profiles for **1Si** after 24h deposition time. Height profiles at 1, 2 and 3 are consistent with crystals of 2-3 MOF layers thickness grafted on the TSP functionalized Si wafer.

ESI-1 crystal structure and SHAPE analysis

S H A P E v2.1 Continuous Shape Measures calculation

(c) 2013 Electronic Structure Group, Universitat de Barcelona

Contact: llunell@ub.edu

OP-8 1 D8h Octagon

HPY-8 2 C7v Heptagonal pyramid

HBPY-8 3 D6h Hexagonal bipyramid

CU-8 4 Oh Cube

SAPR-8 5 D4d Square antiprism

TDD-8 6 D2d Triangular dodecahedron

JGBF-8 7 D2d Johnson gyrobifastigium J26

JETBPY-8 8 D3h Johnson elongated triangular bipyramid J14

JBTPR-8 9 C2v Biaugmented trigonal prism J50

BTPR-8 10 C2v Biaugmented trigonal prism

JSD-8 11 D2d Snub diphenoid J84

TT-8 12 Td Triakis tetrahedron

ETBPY-8 13 D3h Elongated trigonal bipyramid

Structure [ML8]

OP-8 32.380; HPY-8 22.052; HBPY-8 15.339; CU-8 10.667; **SAPR-8 2.109**; **TDD-8 2.650**; JGBF-8 13.592; JETBPY-8 26.274; **JBTPR-8 2.806**; **BTPR-8 1.906**; JSD-8 4.594; TT-8 11.142; ETBPY-8 21.544.

(a)

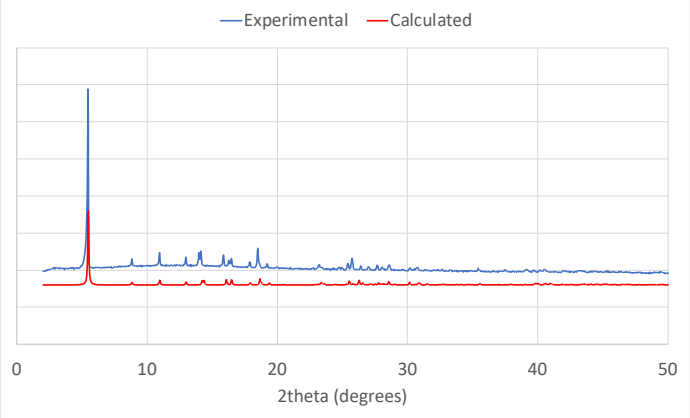

(b)

(c)

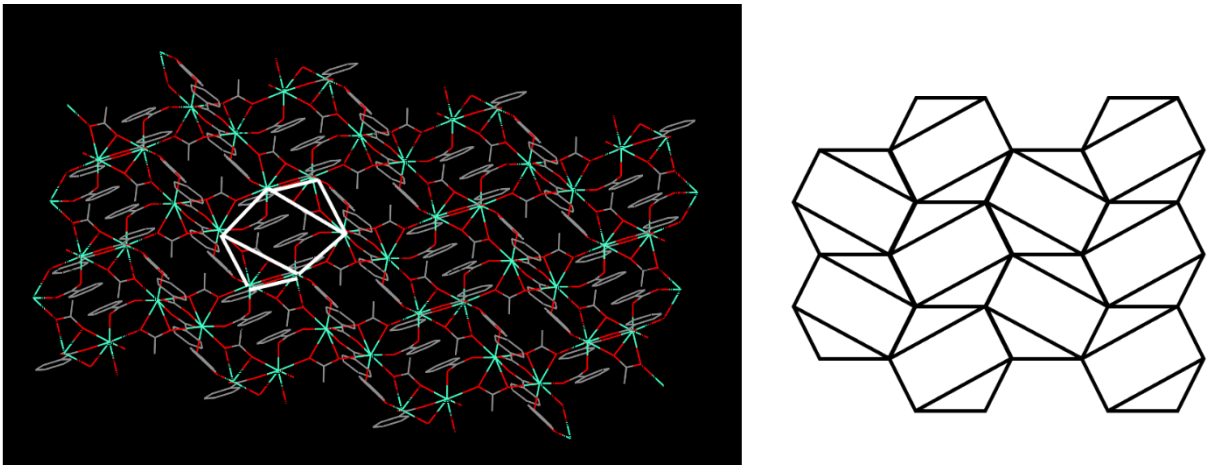

Figure S1. Top view of the 2D layers of **1**. The white lines are just a guide for the eye, to show the three types of Gd-Gd distances within the layer. At right, an idealized topological drawing of the 2D layer of Gd(III) ions in **1**.

ESI-1 Raman spectrum calculations

The Raman spectrum of **1** was simulated from a representative substructure of the 2D MOF, shown in Figure S2. In this calculation the two central Gd(III) atoms were replaced by La(III) to avoid the magnetic interaction between lanthanoid centers. Additionally, the external La(III) ions were transformed into Na(I) ions to keep the charge neutrality at the computed fragment. The Raman spectrum of **1** was computed using the Gaussian09 suite of programs. [1] A single point calculation, including frequencies, was performed employing the B3LYP [2] functional along with the def2-SVPD basis set[3] for all the H, C, O and Na atoms. The La atoms were described using the def2-TZVPP basis set,[3,4] which includes ECPs for these metal centers. Since the structure is not allowed to relax, several negative frequencies appear in this calculation; however, their weight in the simulation is expected to be low and have been ignored for plotting the final Raman spectrum.

References

[1] Gaussian 09, Revision D.01, M. J. Frisch, G. W. Trucks, H. B. Schlegel, G. E. Scuseria, M. A. Robb, J. R. Cheeseman, G. Scalmani, V. Barone, B. Mennucci, G. A. Petersson, H. Nakatsuji, M. Caricato, X. Li, H. P. Hratchian, A. F. Izmaylov, J. Bloino, G. Zheng, J. L. Sonnenberg, M. Hada, M. Ehara, K. Toyota, R. Fukuda, J. Hasegawa, M. Ishida, T. Nakajima, Y. Honda, O. Kitao, H. Nakai, T. Vreven, J. A. Montgomery, Jr., J. E. Peralta, F. Ogliaro, M. Bearpark, J. J. Heyd, E. Brothers, K. N. Kudin, V. N. Staroverov, T. Keith, R. Kobayashi, J. Normand, K. Raghavachari, A. Rendell, J. C. Burant, S. S. Iyengar, J. Tomasi, M. Cossi, N. Rega, J. M. Millam, M. Klene, J. E. Knox, J. B. Cross, V. Bakken, C. Adamo, J. Jaramillo, R. Gomperts, R. E. Stratmann, O. Yazyev, A. J. Austin, R. Cammi, C. Pomelli, J. W. Ochterski, R. L. Martin, K. Morokuma, V. G. Zakrzewski, G. A. Voth, P. Salvador, J. J. Dannenberg, S. Dapprich, A. D. Daniels, O. Farkas, J. B. Foresman, J. V. Ortiz, J. Cioslowski, and D. J. Fox, Gaussian, Inc., Wallingford CT, 2013.

[2] a) S. H. Vosko, L. Wilk and M. Nusair, Accurate spin-dependent electron liquid correlation energies for local spin density calculations: a critical analysis, Can. J. Phys., 1980, 58, 1200-1211, https://doi.org/10.1139/p80-159; b) C. Lee, W. Yang and R. G. Parr, Development of the Colle-Salvetti correlation-energy formula into a functional of the electron density, Phys. Rev. B: Condens. Matter Mater. Phys., 1988, 37, 785-789, https://doi.org/10.1103/PhysRevB.37.785; c) A. D. Becke, Density-functional thermochemistry. III. The role of exact exchange, J. Chem. Phys., 1993, 98, 5648-5652, https://doi.org/10.1063/1.464913; d) P. J. Stephens, F. J. Devlin, C. F. Chabalowski and M. J. Frisch, Ab Initio Calculation of Vibrational Absorption and Circular Dichroism Spectra Using Density Functional Force Fields, J. Phys. Chem., 1994, 98, 11623-11627, https://doi.org/10.1021/j100096a001.
[3] F. Weigend and R. Ahlrichs, Balanced basis sets of split valence, triple zeta valence and quadruple zeta valence quality for H to Rn: Design and assessment of accuracy. Phys. Chem. Chem. Phys. 2005, 7, 3297-3305, https://doi.org/10.1039/b508541a.
[4] a) M. Dolg, H. Stoll, A. Savin and H. Preuss, Energy-adjusted pseudopotentials for the rare earth elements. Theor. Chim. Acta, 1989, 75, 173-194, https://doi.org/10.1007/BF00528565; b) M. Dolg, H. Stoll and H. Preuss, A combination of quasirelativistic pseudopotential and ligand field. Calculations for lanthanoid compounds. Theor. Chim. Acta, 1993, 85, 441-450, https://doi.org/10.1007/BF01112983.

(a)

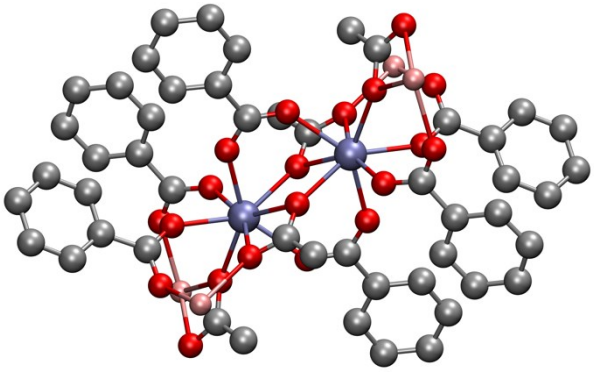

(b)

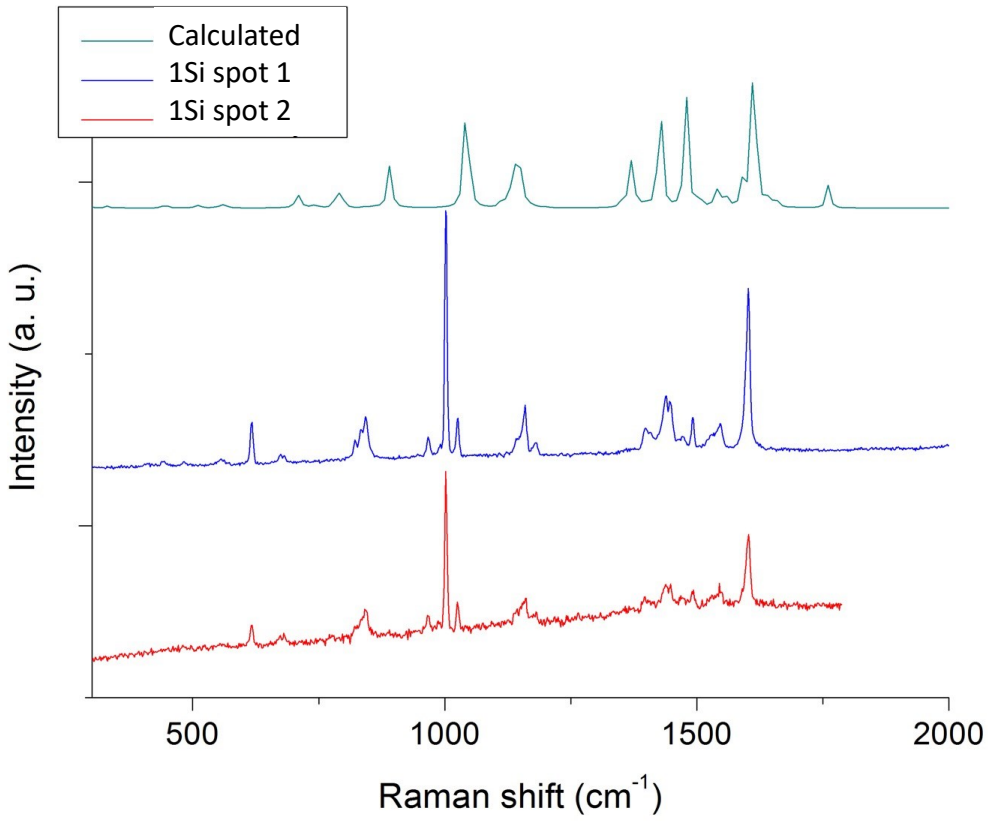

Figure S2. (a) 2D MOF substructure employed to simulate the Raman spectrum (color code: C = gray, O = red, La = blue, Na = pink, H atoms have been omitted for clarity). (b) Raman spectra of **1Si** at different spots, compared to the calculated Raman spectrum for **1**.

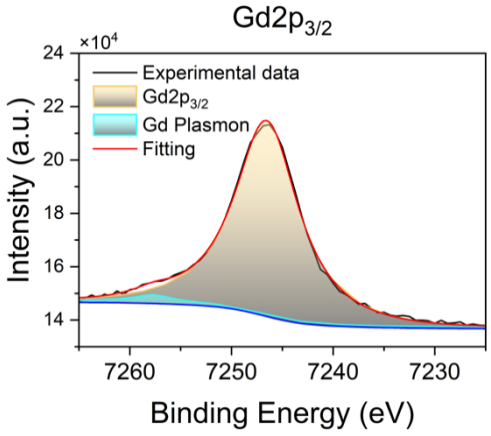

Figure S3. **1Si** HAXPES spectra for the Gd $2p_{3/2}$ core level.

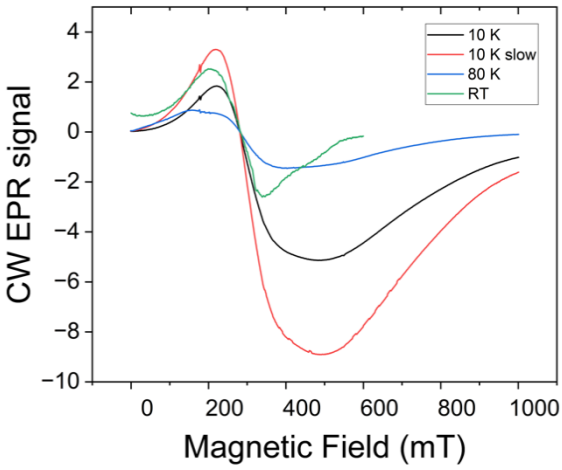

Figure S4. CW X-band EPR spectra of bulk **1** at the indicated temperatures.

ESI-2 High-frequency electron paramagnetic resonance (HF-EPR)

Variable temperature CW HF-EPR spectra of bulk **1**, collected at a frequency of 104 GHz, are shown in **Figure S5**. The Gd(III) ion possesses a $4f^7$ electronic configuration with total spin $S = {}^7/_2$ and orbital angular momentum $L = 0$. At the lowest temperature of 5 K, anisotropic contributions are clearly visible as fine structures in the spectra that spread out from the central $m_S = -½$ to ½ transition (indicated by the vertical dashed line in Fig. S5 at 3.756 T or $g^{eff} = 1.985$) that dominates the spectrum at the highest temperatures.

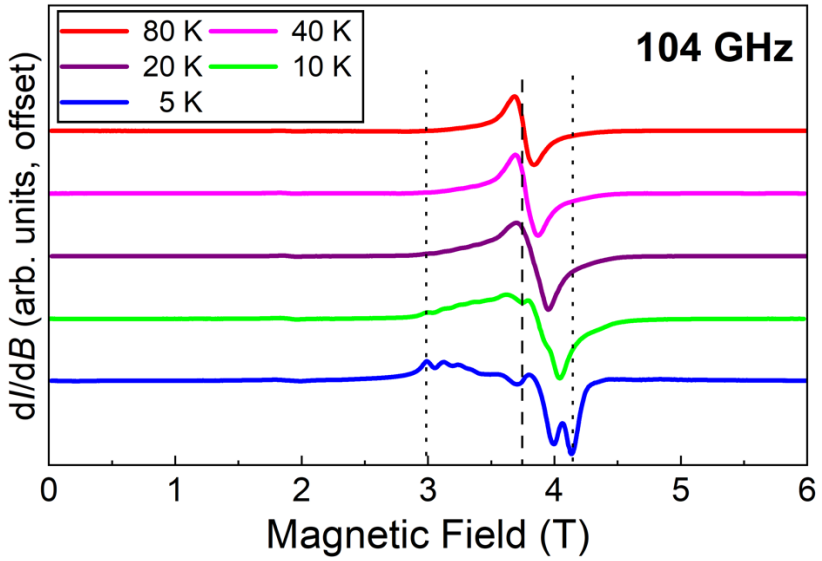

Figure S5: Temperature dependent CW HF-EPR spectra of bulk **1**, recorded at 104 GHz and the temperatures given in the legend. Anisotropic spectral features span from 3.0 to 4.15 T (dotted vertical lines), corresponding to effective *g*-values, $g^{eff} = 2.48$ and 1.79, respectively. The dashed vertical line indicates the central m_S = -1/2 to 1/2 transition at $g^{eff} = 1.985$.

Experimental (black) and simulated (red) 104 GHz HF-EPR spectra are presented in Figure S6 for temperatures of 5 and 80 K. The spin Hamiltonian (SH) employed for the simulations is given in Eq. 1 of the main text. The optimum simulation parameters are: g = 1.985 ± 0.005, D/k_B = -0.167 ± 0.003 K (- 0.117 ± 0.002 cm^{-1}), E/k_B = -0.0043 ± 0.0015 K (- 0.003 ± 0.001 cm^{-1}) i.e., E/D = 0.026.

Due to the absence of first-order orbital momentum, the *g*-tensor components are all expected to be close to the free electron value of 2.00. The relatively broad lines and the fact that it is impossible to simulate all details of the experimental spectra (due to complexities of the exchange, see below) led us to assume an isotropic *g*-tensor. At 80 K, the eight (= 2*S* +1)

sub-levels associated with the $S = {}^{7}/_{2}$ manifold are uniformly populated. Therefore, the relative intensities of the different transitions are dominated by the associated matrix elements, which are strongest for the m_s = 1/2 to -1/2 central transitions.[2] In addition, faster relaxation associated with the anisotropic components at the extremes of the spectra, as well as effects due to exchange (see below), mean that the high temperature results are dominated by the central m_s = 1/2 to -1/2 transitions that do not experience any ZFS.[3] Consequently, the 80 K simulations primarily constrain g = 1.985 ± 0.005. The *D* and *E* parameters are then constrained by the extrema in the spectra (vertical dotted lines). For the perfectly uniaxial case (*E* = 0), these shift from the central transition in a 2:1 ratio. The optimum simulations were thus achieved by tuning *D* and *E* to best match the positions of the outer-most resonances at 5 K. [3] Although the simulations are by no means perfect, they constrain the sign of *D* and provide good estimates for the magnitudes of both *D* and *E*.

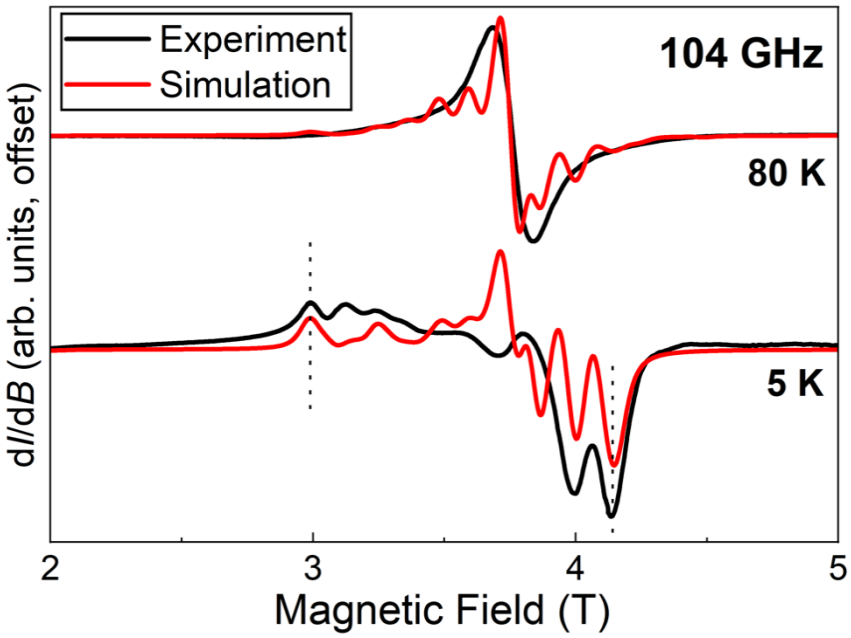

Figure S6: Comparison between experimental 104 GHz HF-EPR spectra and simulations obtained using the spin Hamiltonian of Eq. 1 (main text) at temperatures of 5 and 80 K.

In an attempt to further refine the simulations and to gain insights as to the role of inter-molecular exchange, we tested the simplest possible dimer model for two interacting Gd(III) ions. The 64×64 Hilbert space associated with this model keeps the simulations manageable. Meanwhile, the approach is also justified on the basis that one of the Gd···Gd contacts is: (i) considerably shorter than the others; and (ii) it involves four bridges, as opposed to just 2 and

1 for the other contacts. The multi-spin Hamiltonian (MSH) describing this situation is as follows:

$$\widehat{H} = \sum_{i=1}^{2} \left[\mu_{\mathrm{B}} \boldsymbol{B}_0 \cdot \tilde{\boldsymbol{g}}_i \cdot \hat{\boldsymbol{s}}_i + d_i \hat{s}_{zi}^2 + e_i \left(\hat{s}_{xi}^2 - \hat{s}_{yi}^2 \right) \right] - 2J \hat{\boldsymbol{s}}_1 \cdot \hat{\boldsymbol{s}}_2 .$$

The index i = 1, 2 labels the two Gd(III) ions in the summation, which contains the same local interactions as Eq. 1 (main text); here, lowercase symbols are employed in place of the uppercase ones in Eq. 1 to denote the fact that they refer to individual spins within a dimer, as opposed to the total spin of the dimer (a convention employed extensively in the molecular magnetism literature).[4] As will be seen, we employ the same ZFS and g parameters for both Gd sites as those used for the uncoupled simulations in Fig. S6. The last term in Eq. S1 specifies an isotropic exchange interaction between the two Gd spins, with coupling constant J; note that the $-2J(S_i \cdot S_j)$ convention is used here, where $J > 0$ denotes ferromagnetic (FM) interactions and $J < 0$ antiferromagnetic (AF) ones.

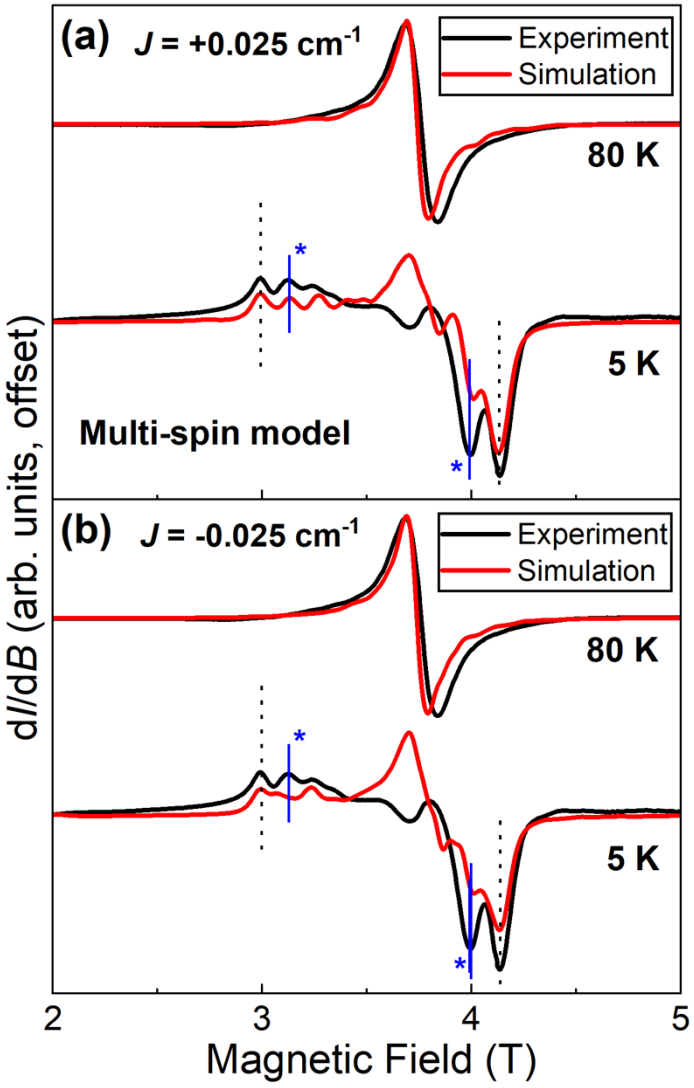

Figure S7 displays two simulations of the 5 and 80 K, 104 GHz spectra using the MSH model, one with FM (a) and the other with AF (b) Gd···Gd coupling of magnitude J = 0.025 cm^{-1}, equal to the value estimated from magnetic measurements. The first thing to note is that this does affect the fine structures seen in the simulated spectra quite considerably (compare to Fig. S6). However, the impact on the outer-most resonance positions (vertical dotted lines) is minimal – a well-known result for the FM case in which the uniform precession frequency is unshifted relative to the single-spin resonance mode frequency.[5] This observation provides further support for the ZFS parameters determined from the simulations in Fig. S6. Most noticeable is the near complete vanishing of fine structures in the central region of the spectrum at 80 K, both for the FM and AF cases. This can be attributed to the increased multiplicity [$(2s + 1)^2 = 64$] of the coupled energy level diagram, which gives rise to many more overlapping/unresolved resonances in the central part of the spectrum, with small relative

shifts brought on by the weak exchange.[6] The net effect is a single broad resonance centered at the average g = 1.985 ± 0.005. The featureless experimental 80 K spectrum therefore supports the existence of weak, albeit measurable intermolecular interactions.

Another consequence of the exchange, which can clearly be seen in the FM case, is the doubling of the periodicity of peaks at the low-field end of the spectrum. This is because the low-energy states approximate those of a giant spin $S = 2s = 7$ dimer, with $2S = 14$ peaks in the parallel portion of the EPR spectrum, as opposed to just $2s = 7$ in the uncoupled case. However, the corresponding axial ZFS parameter for the dimer, $D_d \sim 6d/13$, i.e., roughly half that of the monomer, leading to approximately half the peak spacing.[7] It is noticeable that the uncoupled simulations (Fig. S6) fail to reproduce the strong 2nd peak on the low-field side of the spectrum (marked by an asterisk in Fig. S7), corresponding to the coupled $m_S = -6$ to -5 transition in the FM case. Various other features of the coupled simulations also improve relative to the uncoupled ones, providing further support for intermolecular interactions. However, it is not possible to obtain good agreement in the central portion of the 5 K spectrum. This highlights the oversimplicity of the dimer model. Indeed, if the intermolecular interactions are dipolar in nature, even the form of the MSH is incorrect. Consequently, we prefer not to read too much into either the sign or the precise magnitudes of the couplings employed in the simulations shown in Fig. S7. Our aim here is simply to show that: (i) the ZFS and g parameters obtained from EPR are robust; (ii) intermolecular interactions account for the deviations between the experimental and simulated spectra in Fig. S6; and (iii) the overall findings of the HF-EPR and magnetic studies are in broad agreement.

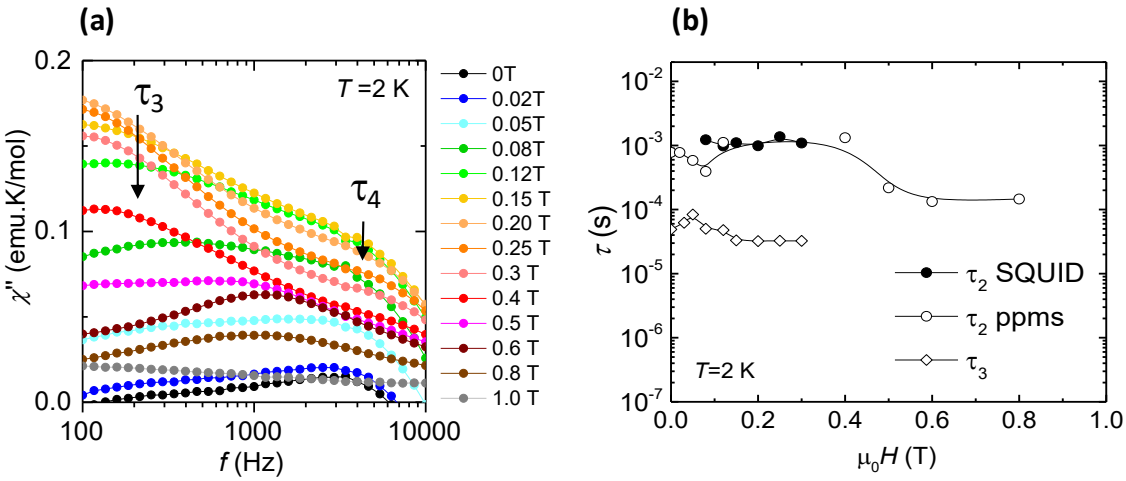

Figure S8. (a) $\chi''(f, H)$ curves measured in the high frequency-region by PPMS at T = 2.0 K and different applied magnetic fields (0-1 T), where the presence of the two relaxation processes τ_2 and τ_3 are is observed; (b) field dependence of the relaxation times $\tau_2(H)$ and $\tau_3(H)$.

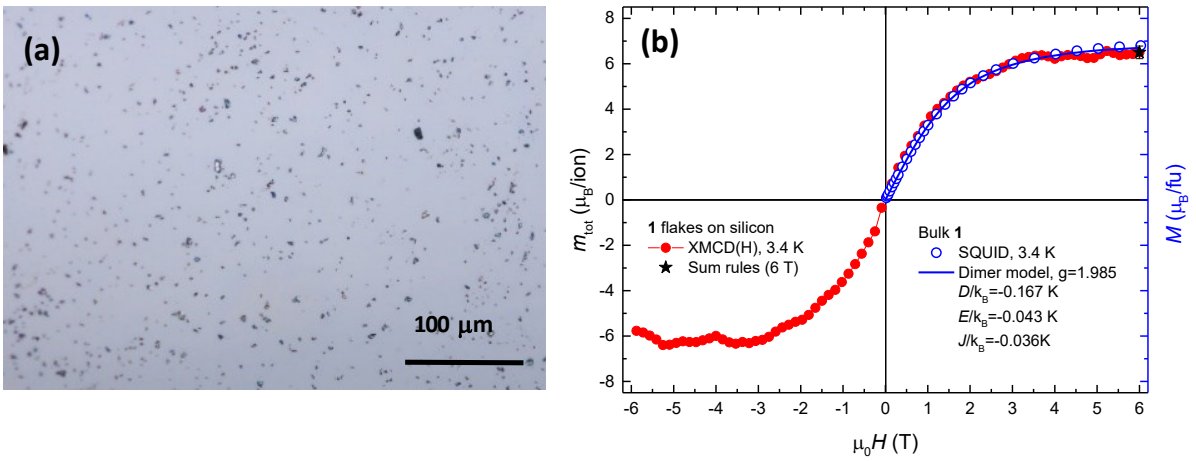

Figure S9. (a) Optical microscopy photograph of Gd 2D MOF flakes deposited on silicon by spin coating; (b) Field-dependence of the total magnetic moment, $m_{tot}(H)$, obtained from XMCD(H); a value m_{tot} = 6.50 ± 0.18 μ_B/ion was obtained from sum rules at 6 T and 3.4 K. Right scale: field-dependence of the magnetization, $M(H)$, measured by SQUID for **1** in bulk at 3.4 K, along with the theoretical curve, calculated within a dimer model at T = 3.4 K with the EPR-obtained values g=1.985, D/k_B=-0.167 K, E/k_B=-0.043 K, J/k_B=-0.036K.

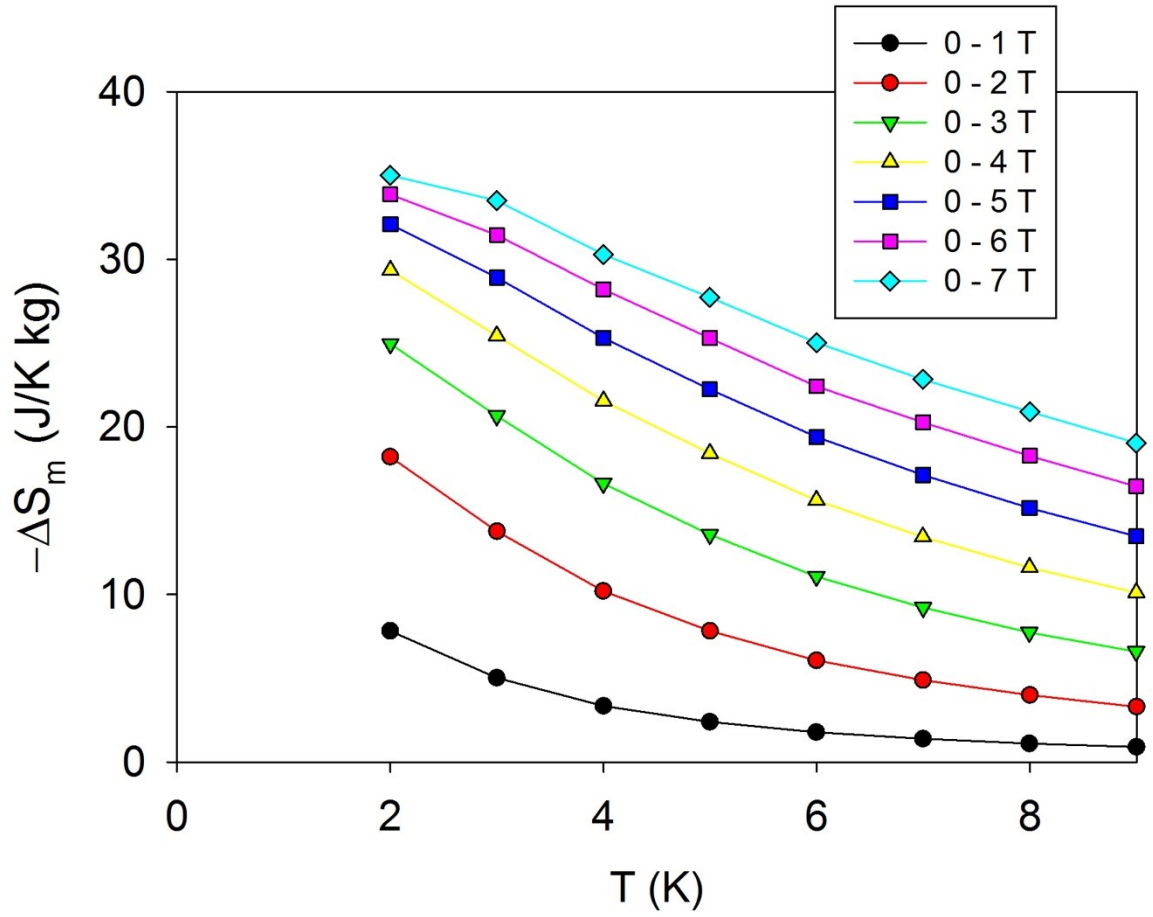

Figure S10. Magnetic entropy change, -ΔS_m, at the indicated field change for **1**.

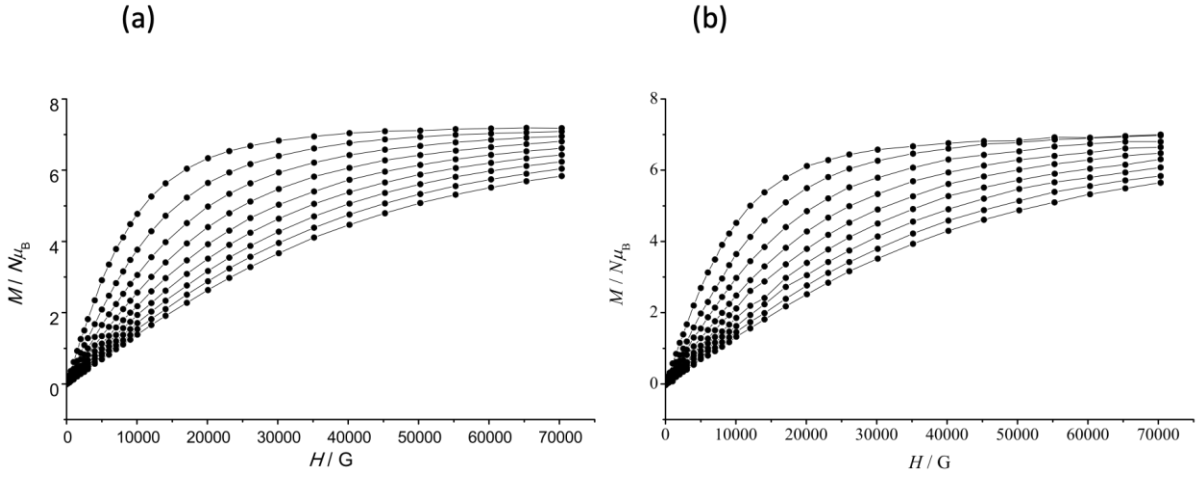

Figure S11. Magnetization vs field as a function of temperature (2 to 10 K) for **1Si,** with the wafer parallel (a) and perpendicular (b) to the SQUD magnetic field.

(a) (b)

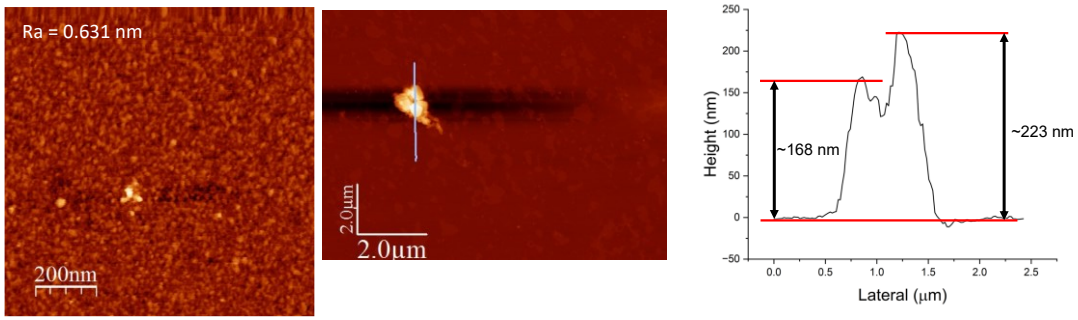

(c)

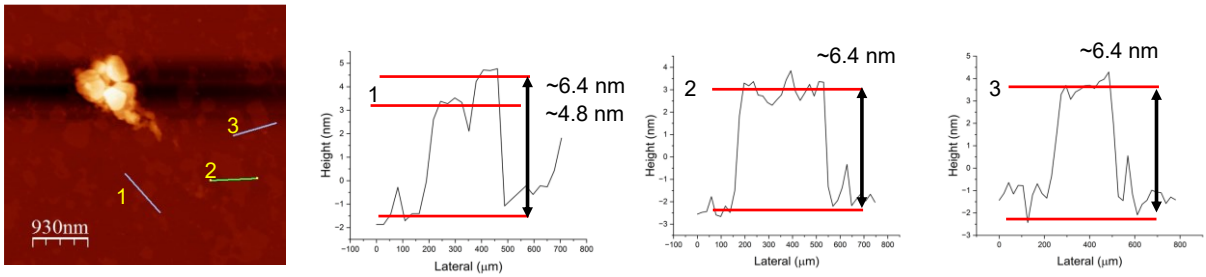

Figure S12. (a) AFM image of **1Si** after 1 hour deposition time. Roughness is indicated in the figure. (b) AFM image and height profile for **1Si** at 24h deposition time., showing some large crystallites grafted on the TSP functionalized Si wafer. (c) AFM image and height profiles for **1Si** after 24h deposition time. Height profiles at 1, 2 and 3 are consistent with crystals of 2-3 MOF layers thickness grafted on the TSP functionalized Si wafer.

References

1 A. Gaita-Ariño, F. Luis, S. Hill and E. Coronado, *Nat. Chem.*, 2019, **11**, 301 – 309.

2 D. Zipse, J. M. North, N. S. Dalal, S. Hill and R. S. Edwards, *Phys. Rev. B*, 2003, **68**, 184408.

3 M. de Souza, S. Reis, D. Stinghen, L. Escobar, R. A. Cassaro, G. Poneti, C. Bortolot, J. Marbey, S. Hill and M. Vaz, *Inorg. Chem.*, 2022, **61**, 12118 – 12128.

4 A. Wilson, J. Lawrence, E.-C. Yang, M. Nakano, D. N. Hendrickson and S. Hill, *Phys. Rev. B*, 2006, **74**, 140403(R).

5 S. Hill, S. Datta, J. Liu, R. Inglis, C. J. Milios, P. L. Feng, J. J. Henderson, E. del Barco, E. K. Brechin and D. N. Hendrickson, *Dalt. Trans.*, 2010, **39**, 4693 – 4707.

6 S. Hill, R. S. Edwards, N. Aliaga-Alcalde and G. Christou, *Science (80-.).*, 2003, **302**, 1015 – 1018.

7 J. Marbey, P.-R. Gan, E.-C. Yang and S. Hill, *Phys. Rev. B*, 2018, **98**, 144433.